Geophysical Research Letters

RESEARCH LETTER
10.1029/2018GL077436

Key Points:
- We showed 3-D mapping of *P* wave azimuthal and radial anisotropic velocity in the Japan subduction zone
- Mantle flow with small-scale convection related to slab subduction explains mantle anisotropy
- An idea of apparent anisotropy shows that Pacific slab anisotropy is mainly attributed to lamination structure and LPO during seafloor spreading

Supporting Information:
- Supporting Information S1

Correspondence to:
M. Ishise,
ishise@eri.u-tokyo.ac.jp

Citation:
Ishise, M., Kawakatsu, H., Morishige, M., & Shiomi, K. (2018). Radial and azimuthal anisotropy tomography of the NE Japan subduction zone: Implications for the Pacific slab and mantle wedge dynamics. *Geophysical Research Letters*, *45*, 3923–3931. https://doi.org/10.1029/2018GL077436

Received 3 FEB 2018
Accepted 10 APR 2018
Accepted article online 23 APR 2018
Published online 7 MAY 2018

Radial and Azimuthal Anisotropy Tomography of the NE Japan Subduction Zone: Implications for the Pacific Slab and Mantle Wedge Dynamics

Motoko Ishise[1], Hitoshi Kawakatsu[1], Manabu Morishige[2], and Katsuhiko Shiomi[3]

[1]Earthquake Research Institute, The University of Tokyo, Tokyo, Japan, [2]Japan Agency for Marine-Earth Science and Technology, Yokohama, Japan, [3]National Research Institute for Earth Science and Disaster Resilience, Tsukuba-shi, Japan

Abstract We investigate slab and mantle structure of the NE Japan subduction zone from *P* wave azimuthal and radial anisotropy using travel time tomography. Trench normal E-W-trending azimuthal anisotropy (AA) and radial anisotropy (RA) with $VP_V > VP_H$ are found in the mantle wedge, which supports the existence of small-scale convection in the mantle wedge with flow-induced LPO of mantle minerals. In the subducting Pacific slab, trench parallel N-S-trending AA and RA with $VP_H > VP_V$ are obtained. Considering the effect of dip of the subducting slab on apparent anisotropy, we suggest that both characteristics can be explained by the presence of laminar structure, in addition to AA frozen-in in the subducting plate prior to subduction.

Plain Language Summary There is increasing importance and interest in seismic anisotropy because it can provide crucial constraints on the lithospheric structure as well as the nature of dynamics of mantle flow. In this study, we performed two types of anisotropic tomography analyses using the same data set and estimated three-dimensional *P* wave azimuthal and radial anisotropy structures beneath NE Japan. These tomography analyses show that mantle wedge of the subduction zone is characterized by E-W-trending azimuthal anisotropy and radial anisotropy with $VP_V > VP_H$. On the other hand, N-S-trending azimuthal anisotropy and radial anisotropy with $VP_H > VP_V$ are shown in the Pacific slab. Assuming flow-induced lattice preferred orientation of mantle minerals, the observed mantle wedge anisotropy can be explained by 3-D mantle flow with small-scale convection. Also, we evaluated the effect of dip of the slab that is anisotropic and carefully considered resulting apparent radial and azimuthal anisotropies in our tomography. Then, the anisotropy in the Pacific slab can be explained by a combination of positive radial anisotropy due to laminar scatterers in the oceanic plate and azimuthal anisotropy frozen-in during the formation of an oceanic plate whose fast direction is parallel to the ancient spreading direction.

1. Introduction

The northeastern (NE) Japan subduction zone (Figure 1) has been extensively studied seismologically from various perspectives including *P* and *S* wave anisotropy. In the early stage of seismic anisotropy study, surface wave analyses suggested that mantle region beneath the Japan islands is characterized by strong radial anisotropy (RA) with $VS_H > VS_V$ (e.g., Aki & Kaminuma, 1963), where VS_H and VS_V refer to wave speeds of horizontally and vertically polarized horizontally propagating *S* wave in a radially anisotropic system (e.g., Kawakatsu, 2016). Yoshizawa et al. (2010) reported remarkable anisotropy with $VS_H > VS_V$ in the whole mantle wedge in the Japan subduction zone via surface wave tomography. On the other hand, a recent full-waveform inversion study showed relatively weak RA in the mantle wedge beneath the study area (Simutė et al., 2016). As to body wave studies, regional variations of *P* and *S* wave anisotropy have been reported. For example, *S* wave splitting studies using local earthquakes reported north-south (N-S)-trending trench parallel weak anisotropy at eastern fore-arc seismic stations and east-west (E-W)-trending trench normal strong anisotropy at western side back-arc side seismic stations (e.g., Nakajima & Hasegawa, 2004; Okada et al., 1995). The N-S-trending and E-W-trending anisotropy were attributed respectively to lattice preferred orientation (LPO) of B-type and A-type olivine caused by the mantle flow due to the slab subduction. On the other hand, *P* wave azimuthal anisotropy (AA) tomography studies (e.g., Ishise & Oda, 2005; Wang & Zhao, 2008) indicated that E-W-trending trench normal anisotropy prevailed in the whole mantle wedge and that the Pacific slab has N-S-trending trench parallel anisotropy; the authors interpreted that the E-W-trending anisotropy is due to LPO of mantle minerals caused by the wedge mantle flow associated with the

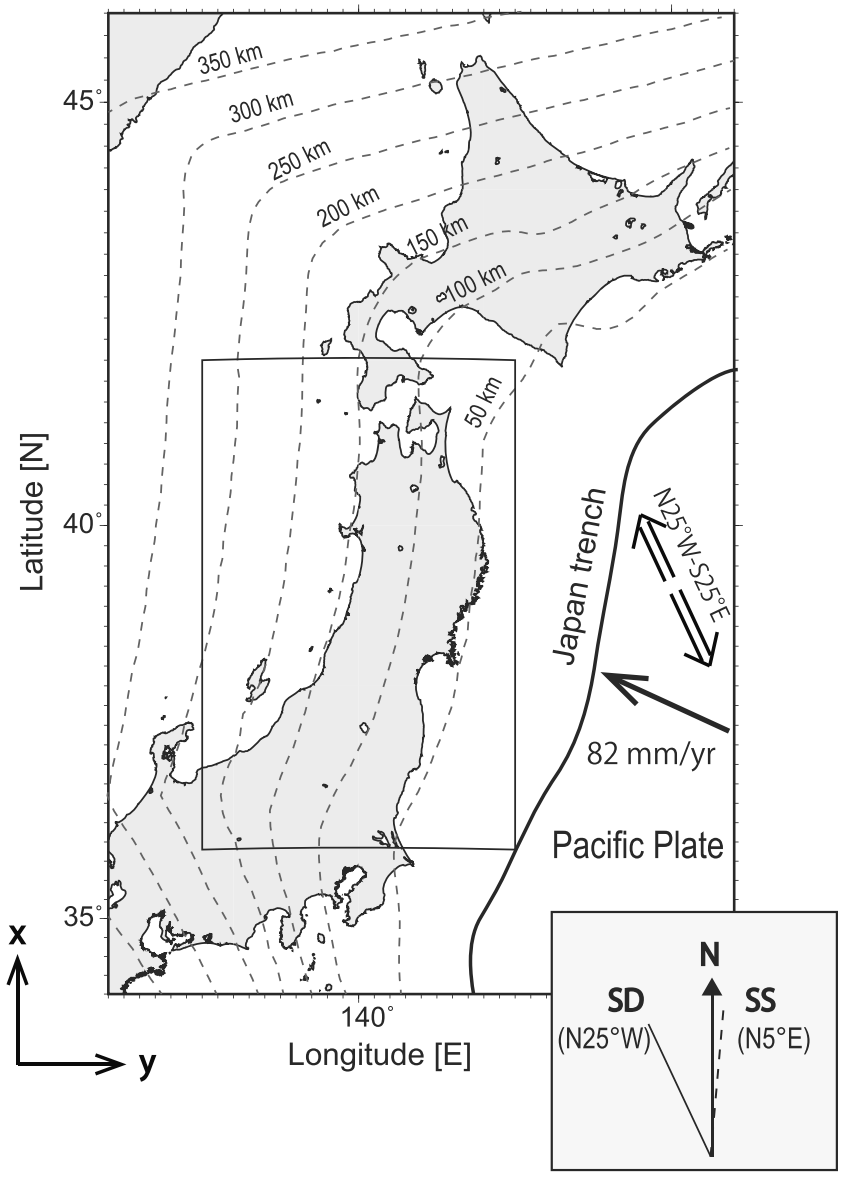

Figure 1. Tectonic setting around northeastern Japan. The broken lines indicate the iso-depth contour of the surface of the subducting Pacific slab (Kita et al., 2010; Nakajima & Hasegawa, 2006). A N25°W–S25°E trending set of arrows represent the ancient spreading direction inferred from the magnetic lineation (Nakanishi et al., 1989), and the thick solid arrow indicates the direction of the plate motion of Pacific plate (Seno et al., 1996). A rectangle shows the study area. The inset summarizes the directions of key features (SS: lab-strike; SD: seafloor-spreading direction). As for the *x*-*y* coordinate at the bottom left, see the caption of Figure 4.

subduction, and the N-S-trending anisotropy is due to the "frozen-in" LPO during the ancient seafloor spreading before subduction.

As indicated above, the features of seismic anisotropy often vary depending on the methods of analysis and the types of data, and there is no unified interpretation for observed anisotropy of the NE Japan subduction zone. In this study, we investigate regional 3-D anisotropic structure beneath NE Japan by means of *P* wave travel time tomography. Assuming that the study area is composed of weakly anisotropic medium with hexagonal symmetry, we estimate 3-D *P* wave azimuthal and radial anisotropic velocity structures separately. By combining two anisotropy tomography results, we then introduce a novel interpretation that differs from previous ones; that is, we discuss mantle wedge anisotropy based on a simulation study of 3-D mantle flow with small-scale convection. Further, we evaluate the effect of dip of the slab that is anisotropic and carefully consider resulting apparent anisotropy by our tomography.

2. Data and Method

We used *P* wave arrival times and locations of earthquakes of Hi-net data (Okada et al., 2004). The earthquakes were selected from local events that occurred in the study area in the period from January to July 2010 and that were observed at more than 20 seismic stations used in this study: A maximum of 285 arrival time data per earthquake are used. We obtained 3,788 earthquakes and 132,282 *P* wave arrival times from 489 seismic stations (Figure S1a in the supporting information). We describe *P* wave anisotropic velocity using parameters assigned to 3-D grid points set in the study area. Grid intervals are set at 0.25–0.3° in the latitudinal and longitudinal directions and 10–30 km in the vertical direction (Figure S1b).

Our anisotropic velocity analyses consist of two stages. In the first stage, a simultaneous inversion of 1-D isotropic *P* wave velocity structure and hypocenter relocation was applied. The 1-D structure routinely used to determine hypocenters at the National Research Institute for Earth Science and Disaster Resilience (Ukawa et al., 1984) was employed as an initial isotropic velocity structure. The resultant 1-D structure and the relocated earthquakes were used as an initial isotropic velocity structure and initial location of the earthquakes in the subsequent 3-D analyses (Figures S1a and S1c). In the second stage, assuming that the study area is composed of weakly anisotropic media with either horizontal or vertical hexagonal symmetry axis, we conducted two kinds of anisotropic tomography analyses: AA and RA tomography in which we used the same seismic data. For the AA analysis, following Ishise and Oda (2005, 2008), we assumed that the symmetry axis is in the horizontal plane and estimated the 3-D distributions of isotropic velocity and anisotropy parameters (direction of symmetry axis and strength of anisotropy). In the RA tomography, we assumed that the symmetry axis is vertical and estimated the strength of anisotropy as well as the 3-D isotropic velocity structure following Ishise and Kawakatsu (2012). The unknown parameters are isotropic velocity perturbation and dimensionless parameter to describe the strength of anisotropy (see Text S1 in the supporting information). It should be noted that the hexagonal symmetry considered here corresponds to that with the elliptic condition (Kawakatsu, 2016; Thomsen, 1986).

3. Result

Figure 2 shows tomography images at a depth of 70 km that present following essential features of seismic structure in the slab and mantle region. Resultant anisotropic tomography images depth of 40 km or deeper (40, 55, 70, 100, and 130 km) are shown in Figures S2 and S3.

3.1. Isotropic Velocity

Both AA and RA tomography inversions show a similar distribution pattern of isotropic velocity: The Pacific slab is basically characterized by high-velocity anomaly, and there exist conspicuous low-velocity anomalies in the mantle wedge above the slab. These isotropic features are familiar characteristics for the study area (e.g., Tsuji et al., 2008; Zhao et al., 1992). The similarity among them suggests that the isotropic velocity terms are suitably resolved in both azimuthal and radial anisotropic inversions. That is, it appears that the present tomography analyses succeeded in separating isotropic and anisotropic terms.

3.2. Azimuthal Anisotropy

In the AA inversion, the Pacific slab is imaged as an N-S-trending AA dominating region—that is, *P* wave traveling in the N-S direction is the fastest in the horizontal plane—and the mantle wedge as an E-W-trending AA dominating region, although NW-SE-trending AA is observed in the mantle wedge south of 37.5°N. The distribution pattern of anisotropy directions is roughly consistent with those reported by previous *P* and *S* wave anisotropy studies (e.g., Ishise & Oda, 2005; Nakajima et al., 2006); the present study, however, does not show trench parallel AA in the fore arc mantle wedge inferred from *S* wave splitting studies.

3.3. Radial Anisotropy

In the radial anisotropic tomography inversion, the Pacific slab is basically characterized by horizontally fast RA; that is, *P* wave speed in the horizontal plane (VP_H) is faster than that along the vertical direction (VP_V) ($VP_H > VP_V$) that is defined as positive RA in this study. In contrast to the Pacific slab, the mantle wedge shows vertically fast (negative) RA. Vertical cross sections indicate these characteristics of slab and mantle anisotropy more clearly (Figure S3). These features of the mantle wedge and slab anisotropy are

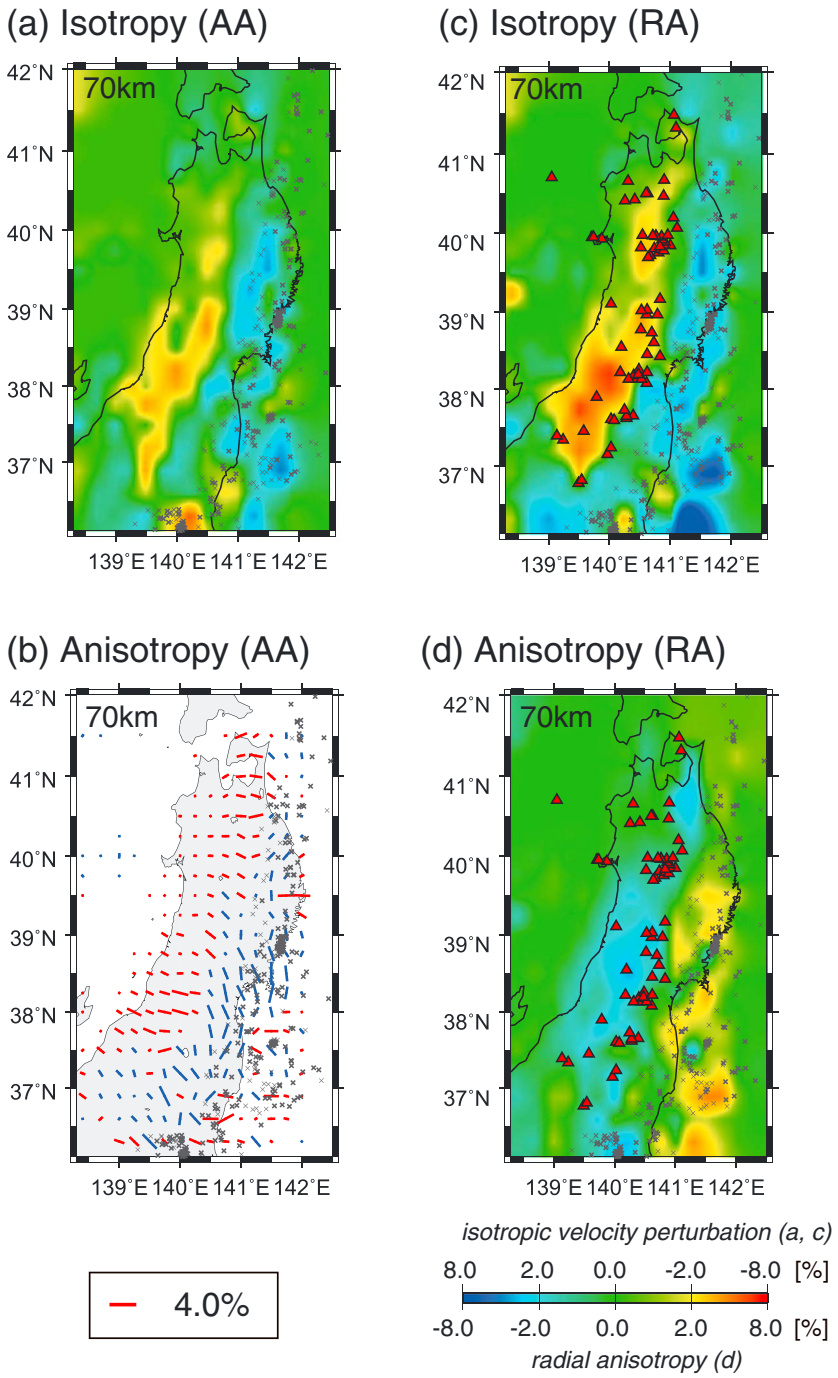

Figure 2. Lateral variations of azimuthal and radial anisotropic velocity at 70 km depth. (a) Isotropic velocity and (b) azimuthal anisotropy obtained by the azimuthal anisotropy tomography. Each bar in (b) represents strength of anisotropy and fast propagation direction by its length and direction, and the color indicates the trend of fast propagation direction: blue for N-S trending and red for E-W trending. (c) Isotropic velocity and (d) radial anisotropy obtained by the radial anisotropy tomography. Isotropic and radial anisotropy velocity perturbations are shown by a color scale at the bottom. The red triangles in (c) and (d) represent active volcanoes.

quantitatively expressed by the depth variation of averaged RA (Figure 3). Similar distribution of *P* wave RA has been estimated by tomography analyses following our previous work, Ishise and Kawakatsu (2012) (e.g., Ishise et al., 2012; Wang & Zhao, 2013). It should be noted that this characteristic of *P* wave RA ($VP_V > VP_H$) is opposite to that of *S* wave RA ($VS_H > VS_V$) of Yoshizawa et al. (2010) based on surface wave tomography.

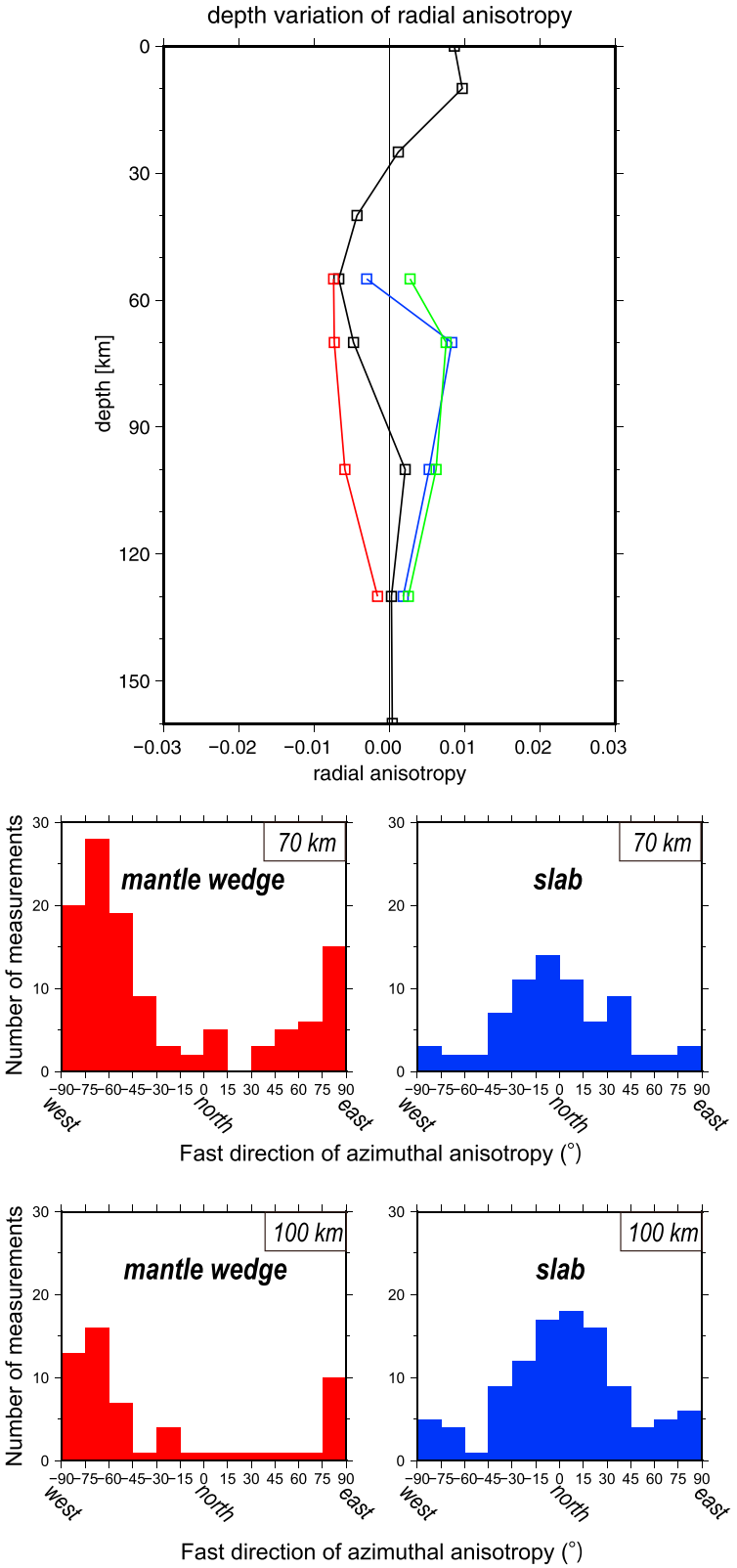

Figure 3. (a) Depth variation of averaged radial anisotropy; black: the whole study area; blue: Pacific slab; red: mantle wedge. We used the distribution of the relocated hypocenters to determine the boundary between the Pacific slab and the mantle. We divided the Pacific slab into two regions by 37.5°N, where the strike of the slab bends. The green line is for the Pacific slab north to 37.5°N. (b) Histograms of fast directions at two depths (70 and 100 km) for the mantle wedge and the Pacific slab; peak fast directions occur for −75° to −60° and −15° to 0° (70 km)/0° to 15° (100 km) bins, respectively.

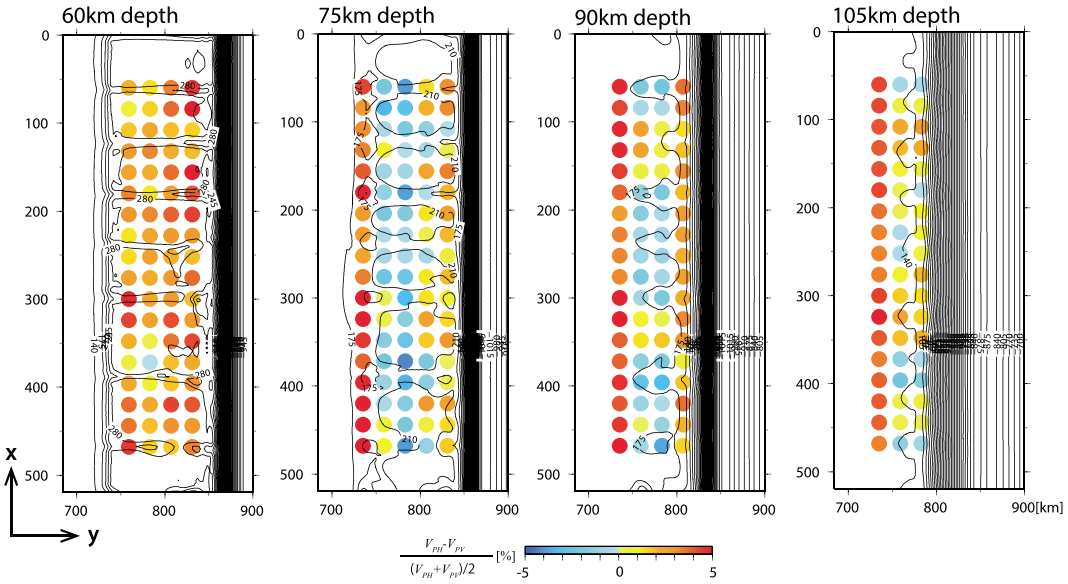

Figure 4. Radial anisotropy predicted by the model of small-scale convection in the mantle wedge (case B1 of Morishige & Honda, 2011). The black lines show contours of temperature anomaly (i.e., deviation from horizontally averaged temperature) every 35 K. The trench is located at y = 990 km, and the direction of plate motion is in the negative y-direction. Three-dimensional distribution of radial anisotropy is estimated from elastic moduli obtained by assuming A-type olivine fabric. The x-y coordinate system used in Morishige and Honda (2011) is indicated at the bottom left. See Figure 1 for the correspondence relationship between the x-y coordinate and location of the study area.

3.4. Resolution of Present Anisotropic Tomography Analyses

Resolution of the anisotropic tomography was checked by the checker-board test (Figures S4 and S5). The distribution patterns of the fast direction of AA, the sign of RA, and isotropic velocity perturbations are well recovered. However, absolute values of isotropic velocity and intensity of azimuthal and RA are poorly recovered. Thus, we deliberately abstain from any quantitative discussion of anisotropic velocity because it might mislead to incorrect conclusions. In addition, we need to take care of the dip angle of the symmetry axis: For example, a previous numerical experiment showed that the AA tomography provided incorrect seismic velocity structure in the case that the symmetry axis dipped steeply (>~60°; Ishise & Oda, 2008).

4. Discussion

4.1. Mantle Wedge Anisotropy

The present tomography analyses show that the mantle wedge of the subduction zone is characterized by E-W-trending AA and negative RA with $VP_V > VP_H$. Here based on the observed anisotropy, we examine 3-D flow in the mantle wedge.

The present *P* wave AA shows good agreement with *S* wave polarization anisotropy in a sense that fast directions generally coincide. This might suggest that seismic anisotropy in the mantle wedge is mainly due to the LPO of A-type olivine (e.g., Ismail & Mainprice, 1998), and the E-W-trending AA prevailing in the mantle wedge suggests that there is a large-scale flow dominating in E-W direction that is likely caused by the subduction of the Pacific plate. Nakajima et al. (2006) suggested that the local slab geometry also affected on the flow in the mantle wedge that might explain the change in the direction of AA at around 37.5°N. Or northwestward subduction of the Philippine Sea plate might disturb the flow field caused by the subduction of the Pacific plate.

Morishige and Honda (2011) numerically investigated the detailed 3-D flow incorporating small-scale convection and resulting seismic anisotropy in the mantle wedge designated for the NE Japan subduction zone (cf. Honda & Yoshida, 2005). They indicated that in horizontal cross sections the flow vector and the fast propagation direction of *P* wave were generally parallel to the plate convergence direction that is consistent with our AA result. They also showed that small-scale convection was composed of narrow and strong (steep slope) down flows and wide and weak (gentle slope) upwellings and the fast propagation direction of *P* wave could tilt vertically around the region (e.g., their Figure 3) that might (especially the down flows) result in

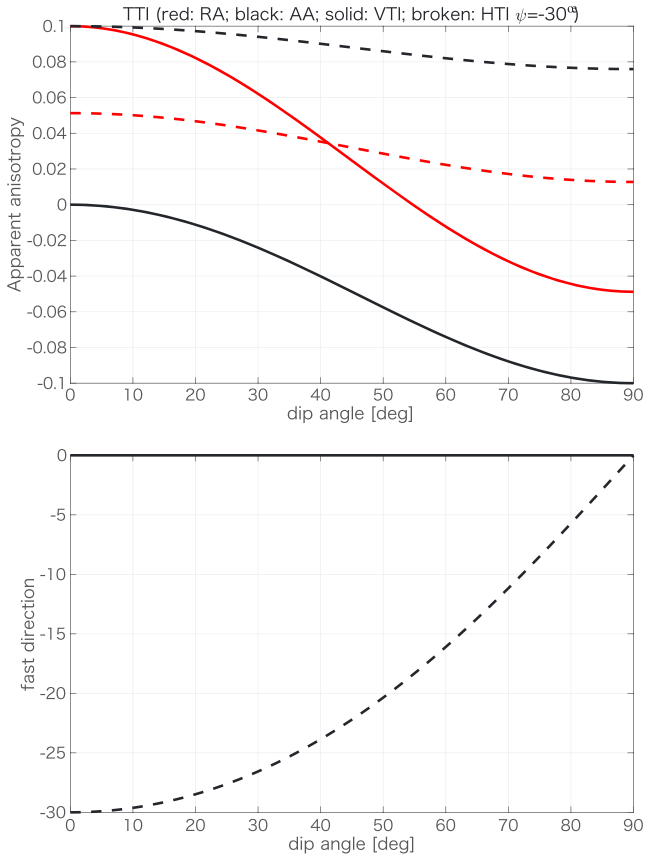

Figure 5. Apparent radial and azimuthal anisotropy expected for dipping TI as a function of dip angle. The solid and broken lines are for cases with original (zero dip) anisotropy given by vertical TI and horizontal TI (fast direction rotated −30° relative to the slab strike). (a) Strength of anisotropy: red for radial anisotropy and black for azimuthal anisotropy. (b) Fast direction measured from the slab strike.

substantial RA. Figure 4 shows the lateral variation of RA estimated from their model. It indicates that negative RA ($VP_V > VP_H$) prevails in the mantle wedge. Since the flow vector is almost horizontal in the mantle wedge with 2-D corner flow (their Figure 3), the mantle wedge without small-scale convection must be characterized by positive RA ($VP_V < VP_H$). Thus, the observation of negative RA may imply the presence of small-scale convection in the mantle wedge beneath NE Japan. Morishige and Honda's numerical simulation indicates that a down flow would produce stronger RA than upwelling because down flow is steeper than upwelling, and therefore, future high-resolution tomography of seismic anisotropy might allow us to identify the flow direction of small-scale convection.

The discrepancy in sign of RA between the present *P* wave tomography ($VP_V > VP_H$) and previous *S* wave studies ($VS_H > VS_V$; e.g., Yoshizawa et al., 2010) might also be attributed to small-scale convection via the difference in resolving power of data used in these analyses. Morishige and Honda's model shown in Figure 4 indicates that positive RA dominates in the shallow portion around a depth of 60 km where strong horizontal shear occurs and negative one in the deeper part corresponding to the convection-cell's core part. Considering that our *P* wave tomography employs many vertical rays, it tends to be more affected by the convection cell's core part with longer raypaths that shows negative anisotropy. Meanwhile, surface waves that traverse the system horizontally are more sensitive to the former structure that is uniform horizontally. Data used in surface wave analyses have periods of a few tens of seconds, while first *P* wave arrival time of local events used in this body wave study has a dominant period of about 1 s at the longest. Therefore, the present *P* wave tomography is also expected to image small-scale anomaly regions that cannot be detected by surface wave analyses.

4.2. Slab Anisotropy

The Pacific slab beneath the NE Japan is characterized by N-S-trending AA and positive RA with $VP_H > VP_V$ (Figure 3). Considering that the slab is dipping with an angle of ~30°, slab anisotropy (azimuthal or radial) obtained in tomography is likely to be apparent one in a sense that it is a projection of true anisotropy onto a horizontal or vertical symmetry framework, and we need to evaluate the effect of dip on obtained anisotropy. The subducting Pacific plate is known to exhibit both AA and RA. Assuming that a hexagonal symmetry as the cause, they may be modeled by transverse isotropy with either a horizontal (HTI) or vertical (VTI) symmetry axis. If we further assume weak anisotropy with elliptic condition (Kawakatsu, 2016; Thomsen, 1986), simple relations between original anisotropy and apparent anisotropy can be derived (see Text S2).

Using the geometrical information given in Figure 1, the possible effect of slab dip on apparent anisotropy can be estimated (Figure 5). If an oceanic plate prior to subduction is characterized by AA of HTI, resulting apparent AA via tomography might be such that the strength is reduced less than 10% and the fast direction rotated less than 5° clockwise (broken black lines in Figure 5). In addition, positive RA (VTI) that exists in the oceanic lithosphere due to laminar scatterers (e.g., Furumura & Kennett, 2005; Kennett & Furumura, 2013; Shito et al., 2013) might introduce apparent AA with about a quarter of the original RA strength with the fast direction parallel to the strike of the slab surface. Kennett and Furumura (2013) estimated the original RA strength of about 1.5%, and thus, this effect (~0.4% anisotropy) may not be so significant, but the effect is to rotate the net fast direction of apparent AA clockwise. So estimated fast directions in Figure 3b that show clockwise rotation (~15°) relative to the fast direction originally existed in the oceanic lithosphere (−30° from the slab strike: Figure 1) may be explained by a combination of these effects.

As to the apparent RA, both HTI and VTI in the oceanic lithosphere contribute to positive apparent RA that is also consistent with the observation (Figure 3a). So observed anisotropy in the slab can be explained by the

seismic anisotropy originally existed in the subducting oceanic plate. It is interesting to note that the situation would be quite different if the slab dip is larger and/or the fast direction of HTI relative to the slab strike is quite different from the present case. As discussed by Song and Kawakatsu (2012, 2013), subduction zone environment can be used to measure seismic anisotropy of the oceanic lithosphere-asthenosphere system, assuming properties do not change significantly with the subduction process.

It should also be noted that the Pacific slab anisotropy might be affected by faults in the slab. Faccenda et al. (2008) suggested that the preferred orientation of bending-related faults existing in the incoming plate cause significant seismic anisotropy. The faults are characterized by near vertical dip and trench-parallel strike that may be modeled as HTI with a trench-normal slow direction that enhances trench-parallel component of HTI caused by LPO that is subparallel to the trench strike in our situation. To what extent this affects HTI might deserve attention, but here we simply assume the dominance of LPO anisotropy for HTI.

4.3. Comparison With Other Anisotropic Tomography

Here we briefly summarize similarities and differences between the present study and the study by Wang and Zhao (2013). Both studies explain anisotropic features in the mantle wedge and slab in terms of the present flow field and past tectonics, respectively. However, although the previous study suggested the existence of B-type olivine in the fore-arc mantle wedge and complexity of the flow field beneath the subduction zone, we carefully discuss seismic anisotropy caused by 3-D mantle flow based on a simulation study of Morishige and Honda (2011). As a result, we found that the resultant mantle wedge anisotropy can be explained by 3-D mantle flow with small-scale convection. As for slab anisotropy, the previous study attributed the difference between the direction of seafloor spreading and that of AA to the coexistence of A-type olivine with B-type olivine. On the other hand, we carefully considered the effect of dip of the slab and indicated that it could introduce the difference.

5. Summary and Conclusions

We performed two types of anisotropic tomography analyses using the same data set and estimated 3-D *P* wave AA and RA structures beneath NE Japan. These tomography analyses show that mantle wedge of the subduction zone is characterized by E-W-trending AA and RA with $VP_V > VP_H$. On the other hand, N-S-trending AA and RA with $VP_H > VP_V$ are shown in the Pacific slab.

Assuming flow-induced LPO of mantle minerals, we considered small-scale convection in the subduction zone, based on a numerical simulation by Morishige and Honda (2011), and discussed 3-D flow in the subduction zone. The observed characteristics of seismic anisotropy in the mantle wedge are consistent with the presence of small-scale convection as suggested by Morishige and Honda (2011). Also, we evaluated the effect of dip of the slab that is anisotropic and carefully considered resulting apparent RA and AA in our tomography. Then, the characteristics of anisotropy in the Pacific slab can be explained by a combination of positive RA due to laminar scatterers in the oceanic plate and AA frozen-in during the formation of an oceanic plate whose fast direction is parallel to the ancient spreading direction.

Acknowledgments
The arrival time data used in this study are picked by the National Research Institute for Earth Science and Disaster Resilience. The lists of earthquakes and seismic stations are available from https://doi.org/10.17632/nxcfcpm6b3.1. The raw data (waveforms) are available from Hi-net (https://hinetwww11.bosai.go.jp/auth/download/cont/?LANG=en). This work was partly supported by Grant-in-Aid Japan Society for the Promotion of Science (JSPS) Fellows and KAKENHI 15K13558, 15H05832, and 17H02948. Comments by M. Faccenda and an anonymous reviewer are constructive.

References

Aki, K., & Kaminuma, K. (1963). Phase velocity of love waves in Japan (Part 1) Love waves from Aleutian shock of march 9, 1957. *Bulletin of the Earthquake Research Institute*, *41*, 243–259.

Faccenda, M., Burlini, L., Gerya, T. V., & Mainprice, D. (2008). Fault-induced seismic anisotropy by hydration in subducting oceanic plates. *Nature*, *455*(7216), 1097–1100. https://doi.org/10.1038/nature07376

Furumura, T., & Kennett, B. L. (2005). Subduction zone guided waves and the heterogeneity structure of the subducted plate: Intensity anomalies in northern Japan. *Journal of Geophysical Research*, *110*, B10302. https://doi.org/10.1029/2004JB003486

Honda, S., & Yoshida, T. (2005). Application of the model of small-scale convection under the islands arc to the NE Honshu subduction zone. *Geochemistry, Geophysics, Geosystems*, *6*, Q01002. https://doi.org/10.1029/2004GC000785

Ishise, M., & Kawakatsu, H. (2012). Toward modeling the anisotropic velocity structure beneath the Japanese subduction zone (1). *2012*. Japan Geoscience Union Meeting 2012, SIT41-SIT01

Ishise, M, Kawakatsu, H., & Shiomi, K. (2012). Revision of the 3-D anisotropic velocity structure of the Japan islands using Hi-net data. Northeastern Japan, Seismological Society of Japan Fall Meeting 2012, B12-B02.

Ishise, M., & Oda, H. (2005). Three-dimensional structure of P-wave anisotropy beneath Tohoku district, northeast Japan. *Journal of Geophysical Research*, *110*, B07304. https://doi.org/10.1029/2004JB003599

Ishise, M., & Oda, H. (2008). Subduction of the Philippine Sea slab in view of P-wave anisotropy. *Physics of the Earth and Planetary Interiors*, *166*(1-2), 83–96. https://doi.org/10.1016/j.pepi2007.11.003

Ismail, W. B., & Mainprice, D. (1998). An olivine fabric database: An overview of upper mantle fabrics and seismic anisotropy. *Tectonophysics*, *296*(1-2), 145–157. https://doi.org/10.1016/S0040-1951(98)00141-3

Kawakatsu, H. (2016). A new fifth parameter for transverse isotropy. *Geophysical Journal International*, *204*(1), 682–685. https://doi.org/10.1093/gji/ggv479

Kennett, B. L. N., & Furumura, T. (2013). High-frequency Po/So guided waves in the oceanic lithosphere: I-long-distance propagation. *Geophysical Journal International*, *195*(3), 1862–1877. https://doi.org/10.1093/gji/ggt344

Kita, S., Okada, T., Hasegawa, A., Nakajima, J., & Matsuzawa, T. (2010). Anomalous deepening of a seismic belt in the upper-plane of the double seismic zone in the Pacific slab beneath the Hokkaido corner: Possible evidence for thermal shielding caused by subducted forearc crust materials. *Earth and Planetary Science Letters*, *290*(3-4), 415–426. https://doi.org/10.1016/j.epsl.2009.12.038

Morishige, M., & Honda, S. (2011). Three-dimensional structure of P-wave anisotropy in the presence of small-scale convection in the mantle wedge. *Geochemistry, Geophysics, Geosystems*, *12*, Q12010. https://doi.org/10.1029/2011GC003866

Nakajima, J., & Hasegawa, A. (2004). Shear-wave polarization anisotropy and subduction-induces flow in the mantle wedge of northeastern Japan. *Earth and Planetary Science Letters*, *225*, 365–377. https://doi.org/10.1016/j.epsl.2004.06011

Nakajima, J., & Hasegawa, A. (2006). Anomalous low-velocity zone and lineament of seismicity along it in the subducting Pacific slab beneath Kanto, Japan: Reactivation of subducted fracture zone? *Geophysical Research Letters*, *33*, L16309. https://doi.org/10.1029/2006GL026773

Nakajima, J., Shimizu, J., Hori, S., & Hasegawa, A. (2006). Shear-wave splitting beneath the southwestern Kurile arc and northeastern Japan arc: A new insight into mantle return flow. *Geophysical Research Letters*, *33*, L05305. https://doi.org/10.1029/2005GL025053

Nakanishi, M., Takami, K., & Kobayashi, K. (1989). Mesozoic anomaly lineations and seafloor spreading history of the northeastern Pacific. *Journal of Geophysical Research*, *94*(B11), 15,437–15,462. https://doi.org/10.1029/JB094iB11p15437

Okada, T., Matsuzawa, T., & Hasegawa, A. (1995). Shear-wave polarization anisotropy beneath the north-eastern part of Honshu, Japan. *Geophysical Journal International*, *123*(3), 781–797. https://doi.org/10.1111/j.1365-246X.1995.tb06890.x

Okada, Y., Kasahara, K., Hori, S., Obara, K., Sekiguchi, S., Fujiwara, H., & Yamamoto, A. (2004). Recent progress of seismic observation networks in Japan -Hi-net, F-net, K-NET and KiK-net. *Earth, Planets and Space*, *56*(8), 15–18. https://doi.org/10.1186/BF03353076

Seno, T., Sakurai, T., & Stain, S. (1996). Can the Okhotsk plate be discriminated from the North America plate? *Journal of Geophysical Research*, *101*(B5), 11,305–11,315. https://doi.org/10.1029/96JB00532

Shito, A., Suetsugu, D., Furumura, T., Sugioka, H., & Ito, A. (2013). Small-scale heterogeneities in the oceanic lithosphere inferred from guided waves. *Geophysical Research Letters*, *40*, 1708–1712. https://doi.org/10.1002/grl.50330

Simutė, S., Steptoe, H., Cobden, L., Gokhberg, A., & Fichtner, A. (2016). Full-waveform inversion of the Japanese islands region. *Journal of Geophysical Research*, *121*, 3722–3741. https://doi.org/10.1002/2016JB012802

Song, T.-R. A., & Kawakatsu, H. (2012). Subduction of oceanic asthenosphere: Evidence from sub-slab seismic anisotropy. *Geophysical Research Letters*, *39*, L17301. https://doi.org/10.1029/2012GL052639

Song, T.-R. A., & Kawakatsu, H. (2013). Subduction of oceanic asthenosphere: A critical appraisal in Central Alaska. *Earth and Planetary Science Letters*, *367*, 82–94. https://doi.org/10.1016/j.epsl.2013.02.010

Thomsen, L. (1986). Weak elastic anisotropy. *Geophysics*, *51*(10), 1954–1966. https://doi.org/10.1190/1.1442051

Tsuji, Y., Nakajima, J., & Hasegawa, A. (2008). Tomographic evidence for hydrated oceanic crust of the Pacific slab beneath northeastern Japan: Implications for water transportation in subduction zones. *Geophysical Research Letters*, *35*, L14308. https://doi.org/10.1029/2008GL034461

Ukawa, M., Ishida, M., Matsumura, S., & Kasahara, K. (1984). Hypocenter determination method of the Kanto-Tokai observational network for microearthquakes. *Research Notes of the National Research Centre Disaster Prevention*, *53*, 1–88.

Wang, J., & Zhao, D. (2008). P-wave anisotropic tomography beneath northeast Japan. *Physics of the Earth and Planetary Interiors*, *170*(1-2), 115–133. https://doi.org/10.1016/jp.pepi.2008.07.042

Wang, J., & Zhao, D. (2013). P-wave tomography for 3-D radial and azimuthal anisotropy of Tohoku and Kyushu subduction zone. *Geophysical Journal International*, *193*(3), 1166–1181. https://doi.org/10.1093/gji/ggt086

Yoshizawa, K., Miyake, K., & Yomogida, K. (2010). 3D upper mantle structure beneath Japan and its surrounding region from inter-station dispersion measurements of surface waves. *Physics of the Earth and Planetary Interiors*, *183*(1-2), 4–19. https://doi.org/10.1016/j.pepi.2010.02.012

Zhao, D., Hasegawa, A., & Horiuchi, S. (1992). Tomographic imaging of P and S wave velocity structure beneath northeastern Japan. *Journal of Geophysical Research*, *97*(B13), 19,909–19,928. https://doi.org/10.1029/92JB00603